Available online at www.sciencedirect.com
SCIENCE DIRECT®
Journal of Power Sources 125 (2004) 246–255
JOURNAL OF POWER SOURCES
www.elsevier.com/locate/jpowsour

Thin electrodes based on rolled Pb–Sn–Ca grids for VRLA batteries

A. Caballero, M. Cruz, L. Hernán, J. Morales*, L. Sánchez

Departamento de Química Inorgánica e Ingeniería Química, Facultad de Ciencias, Campus Universitario de Rabanales, Edificio Marie Curie, Universidad de Córdoba, 14071 Córdoba, Spain

Received 15 April 2003; received in revised form 24 July 2003; accepted 28 July 2003

Abstract

Electrodes 0.5 mm thick (i.e. much thinner than conventional ones) and suitable for lead-acid batteries were prepared by using a special pasting procedure that allows plate thickness to be readily controlled. Novel rolled grids of Pb–Sn–low Ca alloys (0.35 mm thick) were used as substrates. Preliminary galvanostatic corrosion tests of the grids revealed an increased corrosion rate relative to conventional casted grids of Pb–Sn alloys (1 mm thick). Cells made with these thin electrodes were cycled under different discharge regimes and the active material at different charge/discharge cycling stages was characterized by X-ray diffraction (XRD), scanning electron microscopy (SEM) and chemical analysis. At a depth of discharge (DOD) of 100%, the cell exhibited a premature capacity loss after the fifth cycle and delivered only a 20% of its nominal capacity after the 10th. By contrast, cycling performance of the electrode was significantly improved at a DOD of 60%. The capacity loss observed at a DOD of 100% can be ascribed to a rapid growth of $PbSO_4$ crystals reaching several microns in size. Such large crystals tend to deposit onto the grid surface and form an insulating layer that hinders electron transfer at the active material/grid interface. For this reason, the cell fails after few cycles in spite of the high PbO_2 content in the positive active material (PAM). On the other hand, at 60% DOD the submicronic particles produced after formation of the PAM retain their small size, thereby ensuring reversibility in the $PbO_2 \Leftrightarrow PbSO_4$ transformation.

Keywords: Thin electrodes; Rolled gold; Lead-acid batteries

1. Introduction

Since its invention more than 150 years ago, and despite its limited storage energy per unit weight, the lead-acid battery has been the most successful electrochemical energy storage system on the market. Although the basic process has changed little in concept, manufacturing methods continue to bring improvements in energy density life and reliability, which are the origin of its permanent leading position on the commercial battery market. The current trend to smaller, lighter devices has opened up new prospects for lead-acid batteries. Meeting these challenges entails a dramatic reduction in battery weight while preserving the ability to deliver very high currents. This is the goal of the battery based on Thin Metal Film (TMF®) Technology developed by Bolder Technologies [1–3]. This type of battery is made from lead foil 0.07 mm thick, so the total thickness of the electrode is approximately 0.25 mm. Unfortunately, this novel, attractive alternative has not yet been made commercially available because of two major degradation problems, namely, (i) the high corrosion rate of the lead foil and (ii) dendrite formation between the electrodes. These two shortcomings combine to result in premature failure of the battery.

A high power VRLA battery was recently reported [4]. Worth special mention among the novelties introduced is a substantial reduction in electrode thickness, from about 1 mm (present values) to approximately 0.5 mm once pasted. Corrosion problems increase as the thickness of the lead strips is reduced. The use of highly corrosion-resistant alloys somehow alleviates this problem. In this context, Pb–Sn–Ca alloys integrate the latest trends in lead alloys combining improved conductivity and mechanical strength [5]. Moreover, rolled Pb–Sn–Ca alloys exhibit a very much finer grain structure, which results in further improved mechanical properties [6]. In this work, we developed thin electrodes by using a novel controlled pasting method that employs a special roller and rolled grids of reduced thickness (∼0.35 mm)

* Corresponding author.
E-mail address: iq1mopaj@uco.es (J. Morales).

0378-7753/$ – see front matter © 2003 Elsevier B.V. All rights reserved.
doi:10.1016/j.jpowsour.2003.07.005

as substrate. The coatings thus obtained were characterized in textural and structural terms, and the electrochemical properties of the resulting cells were determined.

2. Experimental

Positive plates were prepared by mixing lead oxide supplied by S.E.A. Tudor (Exide Technologies), with water, sulfuric acid and fiber, according with the conventional formulation in the manufacture of SLI batteries. Thin rolled grids of Pb–Sn (1.14%)–Ca (0.027%) alloys—dimensions: 40 mm × 75 mm, 0.35 mm thick—were used as current collectors. Plates were obtained by applying the paste manually, using a roller specially designed for this purpose (Fig. 1). It consists of two cylinders, the distance between which can be adjusted to the desired electrode thickness. With the aid of a crank, the cylinders are rotated in opposite directions; by passing the plate through them, one obtains an electrode of controlled thickness. The final thickness of electrodes obtained under these conditions was 0.5 mm (i.e. much smaller than commonly reported values [7]). In order to avoid the contact between the active material and the cylinder surface, and hence the loss of material, the pasted plate was coated with pasting paper 0.23 mm thick supplied by Bernard Dumas S.A. Curing was done for 2 days at 55 °C at a relative humidity about 98%. The plates were then dried in air at 55 °C for 1 day. Standard negative plates prepared with casted grids were supplied by Tudor-Exide; separators (0.8 mm thick) were also obtained from Bernard Dumas. A sulfuric acid solution of specific gravity 1.28 at 15 °C was used as electrolyte in all measurements. The nominal capacity of the cells calculated from dry weight paste was 1.0 Ah (typical benchmark of 8.5 g/Ah). The algorithm used for the plate formation was the following: charging 8 h at *C*2 rate and then charging 12 h at *C*5 rate. Thus, the quantity of electricity which has passed through the plates during formation was 6 Ah (600% of the nominal capacity). The most salient characteristics of the cells are summarized in Table 1.

Corrosion measurements of the grid were made under constant-current conditions. Corrosion products were removed from the corroded grid by dissolution in a boiling solution of sodium hydroxide, manitol and hydrazine, after which the grids were rinsed with water, dried and weighed. The corrosion rate of the grid was calculated from periodically acquired weight loss data.

Table 1
Main characteristics of the cell

	Positive plate	Negative plate
Source	Lead oxide	Conventional negative formulation
Paste density (g/cm^3)	4.0	4.3
Dry paste weight (g per plate)	9.0	13.3
Substrate	Rolled grid (0.35 mm)	Casted grid (0.7 mm)
Number of plates (+/−)	1/2	1/2
Separator type	BD 9023 XP + BD 6080 XP	

Phases were identified, and composition and morphology determined by combining X-ray powder diffraction (XRD), chemical analysis and scanning electron microscopy (SEM). The formation and all electrochemical tests were carried out with a Solartron 1470 A battery tester.

3. Results and discussion

3.1. Influence of DOD on battery life

Table 2 shows the positive active material (PAM) composition as determined using the Peaks® method [8] and chemical analysis. The major phase present after curing for 2 days was α-PbO, followed by $3PbO{\cdot}PbSO_4$ (3BS) and lead. The particle morphology is shown in Fig. 2a. The paste consists of agglomerates of submicronic particles of irregular morphology and ill-defined shape. After formation, the main component was β-PbO_2 (see Fig. 3a). SEM images (Fig. 2b) revealed a change in morphology and particle shape. Thus, particles tended to have a round shape typical of active β-PbO_2. In addition to the reflections for the lead dioxide, a peak at 28.60° 2θ was detected that could be assigned

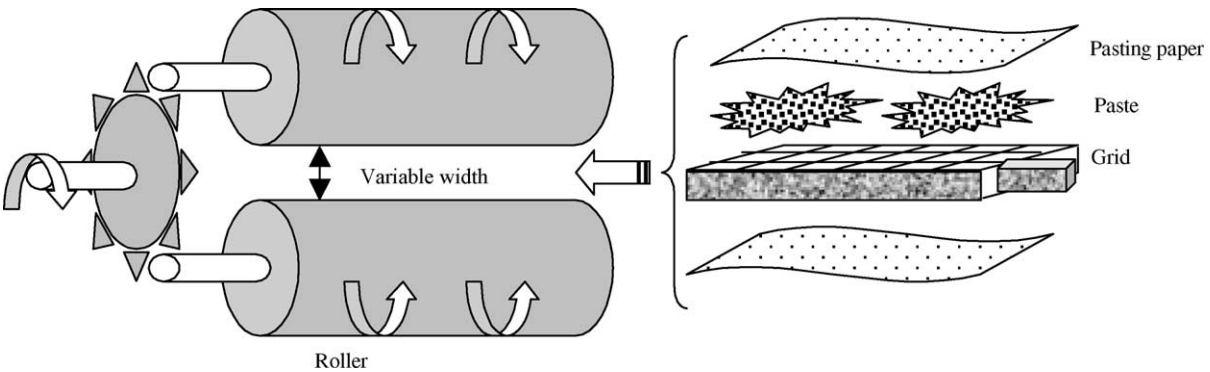

Fig. 1. Main components of the manual pasting device.

Table 2
Phase composition of PAM before and after formation (wt.%)

	β-PbO_2	$PbSO_4$	α-PbO	Pb	3BS
Paste 1	–	–	61	6	32
Formation (OC 400%)[a]	60 (55)	10	30	–	–
Formation (OC 600%)	70 (68)	10	20	–	–
Formation (OC 900%)	68 (65)	10	22	–	–

Values in parentheses are chemical analysis results.
[a] OC: overcharging conditions.

to the strongest line for either α-PbO or α-PbO_2 [9]. Two results are consistent with the presence of α-PbO. Thus, the chemical analysis for Pb^{4+} was virtually coincident with the amount of PbO_2 calculated from the X-ray data. Also, the shoulder on the right of the peak centered at 49.08° 2θ is better assigned to α-PbO rather than to α-PbO_2. In fact, this latter phase exhibits a peak with a somewhat smaller spacing that should have appeared on the left of the β-PbO_2 signal. In our opinion, the identification of α-PbO_2 in PAM from the analysis of a unique reflection (viz. that of maximum intensity at 28.60° 2θ) may lead to spurious conclusions [10]. Both α-PbO and $PbSO_4$ particles were difficult to detect in SEM images obtained from the paste. On the other hand, submicronic particles with well-defined prismatic morphology were clearly seen on the grid surface (see Fig. 2c). This crystal shape is typical of lead sulfate, a phase that was fully confirmed by XRD measurements. Overcharging the cell up to 600% seems the best choice as regards the degree of conversion. This parameter hardly changes if the cell is overcharged to 900%; however, if the overcharge reaches 400%, the degree of conversion decreases (see Table 2).

Preliminary cycling tests were carried out by pasting the grid on one side. The cell performance obtained at a depth of discharge (DOD) 100% is shown in Fig. 4. Under these conditions, cell capacity gradually faded on cycling. Performance was somewhat improved if the grid was pasted on both sides (see Fig. 4), so this configuration was adopted for subsequent measurements. After the fifth cycle, however, the discharge capacity declined and after the 10th, the capacity delivered hardly exceeded 30% of the total value.

Contact between PAM and the grid might have resulted in incomplete formation and capacity fading on cycling. One common way of increasing effective contact between cell components is to increase the number of plates within the cell. We followed an alternative procedure using a variable number of polytetrafluoroethylene pieces. Three compression values (5, 30 and 50%) were tested. The behavior of the cells is depicted in Fig. 5. Even though a small improvement the cell performance was observed as compression was increased, the cells continued to exhibit the same problem; namely a fading capacity after the first few cycles. A final test was conducted to overcome the poor electrochemical response of these thin electrodes by overcharging the plate

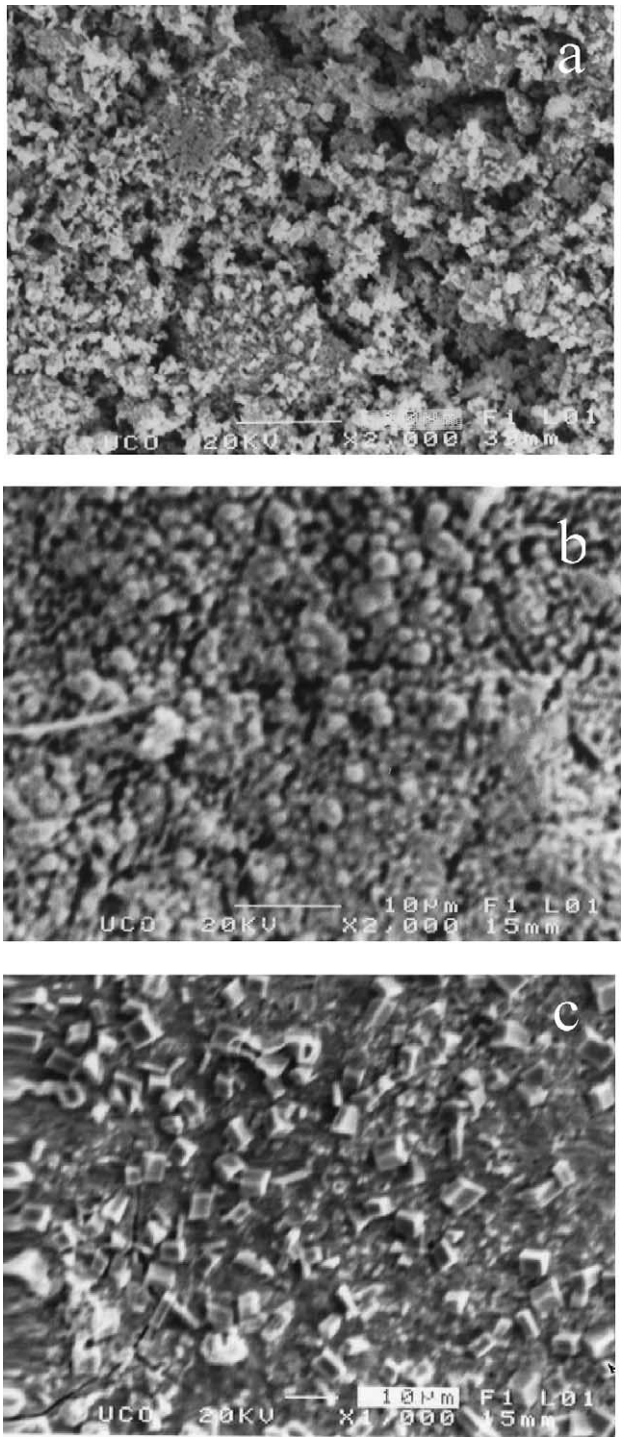

Fig. 2. SEM images: (a) cured paste; (b) paste after formation; (c) grid surface after formation.

to 900%. Clearly, this formation scheme is severely harmful for the electrode (see Fig. 4).

The origin of the reduced capacity observed under high overcharging conditions must be excessive grid corrosion (and the consequent poor adhesion between the active material and the grid) caused by overcharging. Fig. 6 illustrates

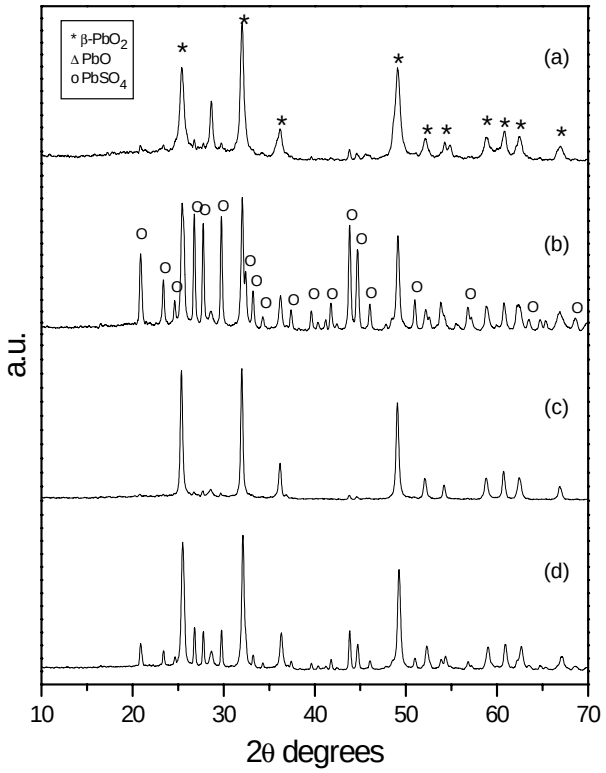

Fig. 3. XRD patterns for PAM after: (a) formation (OC 600%), (b) fifth discharge at 100% DOD, (c) 10th discharge at 100% DOD, and (d) 10th discharge at 60% DOD.

the galvanostatic corrosion tests performed on thin rolled grids at different, constant currents per grid. For comparison, the corrosion behavior of casted grids for conventional SLI batteries (Pb: 1.28% Sn alloy, 1 mm thick) is also shown. Under the same, constant current conditions, the thin rolled grids exhibited higher rate of corrosion. The origin of this difference in reactivity must be differences in the microstructures obtained under the two casting conditions or the presence of Ca in the rolled grid. In fact, the alloys that contain Ca corrode more easily than those which do not. In addition to decreasing grid thickness, the rolling process produces a finer grain structure and a more undulating surface that enhances reactivity, thus promoting an increased weight loss through corrosion. By contrast, in casted grids, which are thicker, the attack is mitigated by the coarse grains that constitute the alloy and by a smoother surface (see Fig. 7a and c). Fig. 7b and d show the morphology of the attacked rolled and casted grids after removal of corrosion products. Although the grid surfaces were clearly altered in both cases the thin rolled grid was more severely degraded. The surface exhibited highly abundant cracks probably formed along grain boundaries. These deep crevices facilitate corrosion in the bulk and result in cell failure. In any case, the grids exhibited a low rate of corrosion at constant currents below 0.125 A (the normal conditions for the cycling tests).

Owing to the difficulty of achieving good electrode performance under deep cycling conditions, the cells were cycled according to the IEC 896-2 specification, using 60% DOD discharges and recharges amounting to 110% of the previous ones. These testing conditions agree with the project performance targets [4] and resulted in clearly improved cycling properties of the electrodes (Fig. 8). One plausible explanation for this favorable effect on the cell chemistry was derived by combining XRD and chemical analysis results with SEM images for the plates at different cycling stages. Fig. 3b–d show some illustrative XRD patterns and Table 3

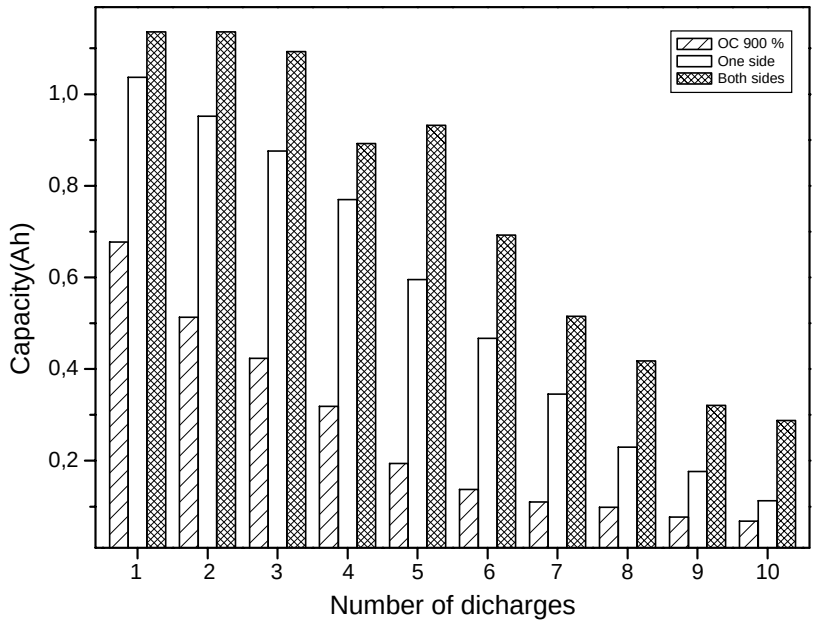

Fig. 4. Plot of capacity vs. cycle number. Tests were performed under different conditions (100% DOD).

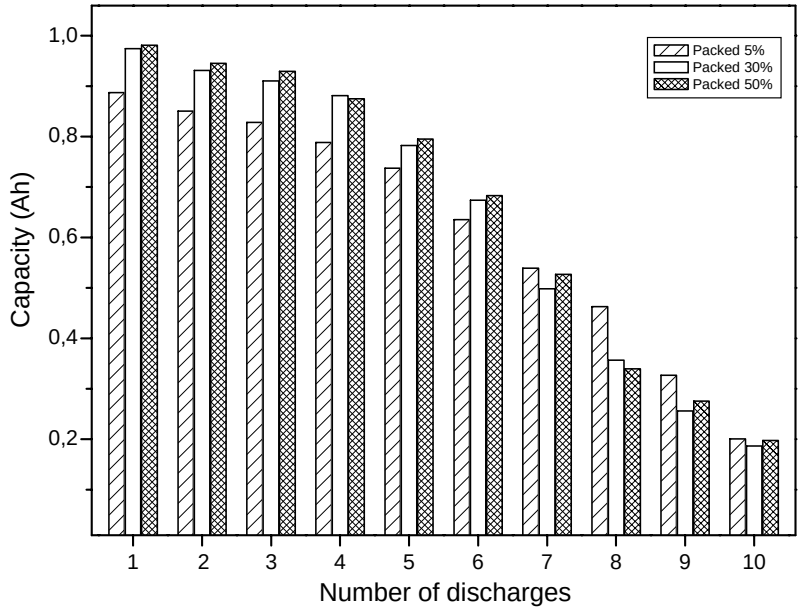

Fig. 5. Influence of compression degree on the cycling properties of the electrodes (100% DOD).

the amount of each phase detected. As can be seen, at 100% DOD the electrode half-reactions:

$$PbO_2 + SO_4^{2-} + 2H^+ + 2e^- \Leftrightarrow PbSO_4 + 2H_2O$$

developed rather satisfactorily (at least over the first five cycles) even though total conversion was not achieved. These results are consistent with the findings of Pavlov and Petkova [11] that not all PAM sites are active towards the electrochemical reaction. However, the predominant phase at the 10th cycle was PbO_2, irrespective of the charge state of the electrode (Fig. 3c). In fact, the PbO_2 content of both discharged and charged plates had increased relative to the starting material, mainly because PbO not converted in the formation step had been gradually transformed into PbO_2. However, on discharging the cell, its conversion to $PbSO_4$ was kinetically hindered. This accounts for the capacity fading on cycling. By contrast, when the cell was cycled to a DOD of 60%, the PbO_2 content of the plate, as expected, shifted depending on the charge state. At the 10th discharge (Fig. 3d), the reduction of PbO_2 to $PbSO_4$ proceeded to an

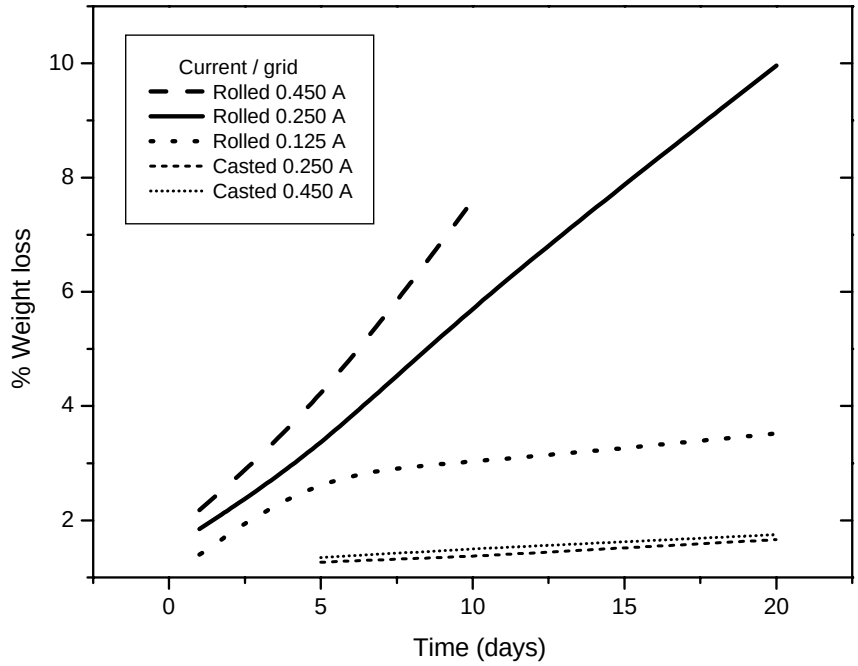

Fig. 6. Results of the galvanostatic corrosion tests.

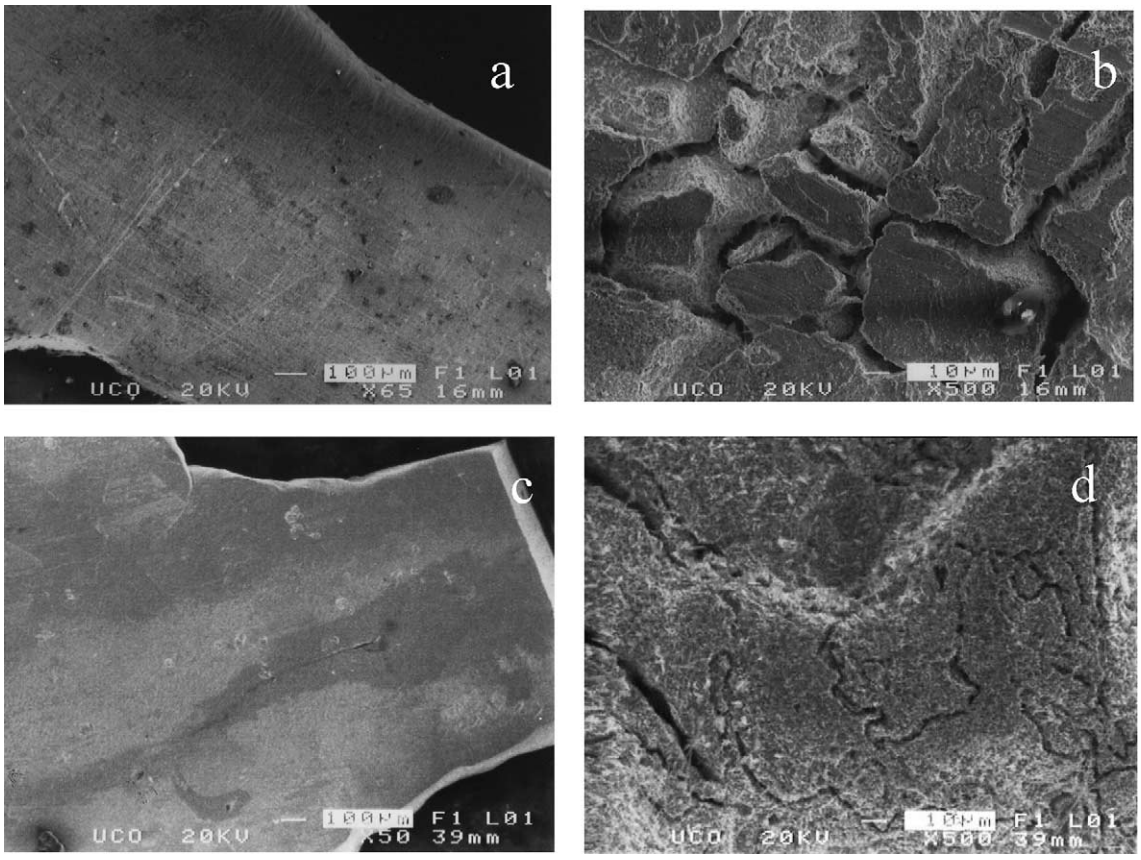

Fig. 7. SEM images of the galvanostatic corrosion tests on rolled (a, b) and casted grids (c, d). (a, c) and (b, d): before and after the treatment, respectively. Experimental conditions: current, 0.25 A/grid, 20 days.

extent highly consistent with the nominal capacity delivered, taking into account the errors inherent in the XRD phase composition method. In any case, the electrode capacity was retained upon extended cycling (Fig. 8). Also, the PbO phase was gradually oxidized and was virtually negligible (<5% as determined by XRD analysis) by the 10th charge.

SEM images shed some light on the influence of the discharge depth on the cycling behavior. For this study, we used

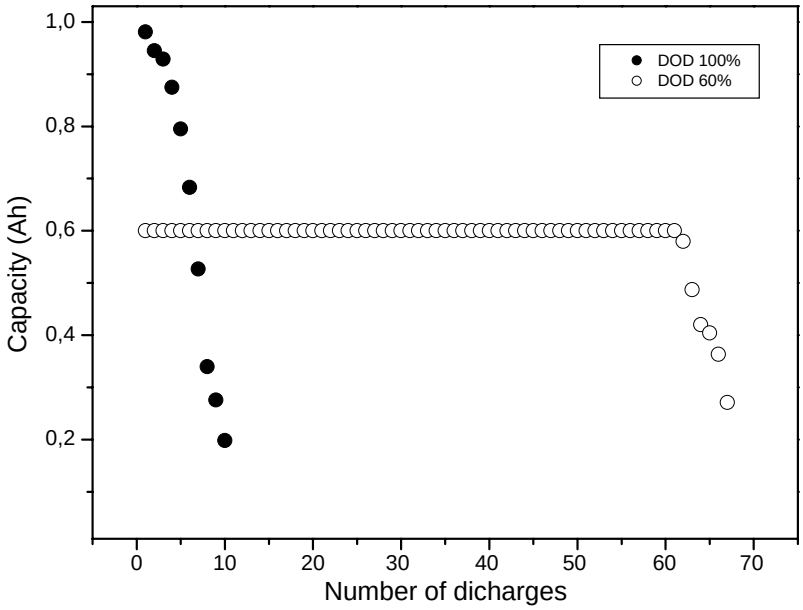

Fig. 8. Influence of DOD on the cycling properties of the electrodes.

Table 3
Phase composition of PAM under different cycling conditions (plate overcharged by 600%)

	β-PbO_2	α-PbO	$PbSO_4$
DOD 100% – C_8—first discharge	8	6	86
DOD 100% – C_8—fifth discharge	24	<1	75
DOD 100% – C_8—fifth charge	72	3	25
DOD 100% – C_8—10th discharge	87	3	10
DOD 100% – C_8—10th charge	89	3	8
DOD 60% – C_5—10th discharge	48	3	49
DOD 60% – C_5—10th charge	88	4	8

cells at the fifth cycle (where the capacity started to decline at 100% DOD, Fig. 4) and at the 10th cycle (the capacity delivered by the cell cycled at 100% DOD was less than 20%, where as that delivered by the cell cycled at a DOD of 60% was retained) (Fig. 8). This set of images was obtained from plates charged and discharged at two different grid positions namely: (i) the grid itself, once washed with distilled water and ethanol (in this case, a compact coating firmly adhered to the surface and capable of withstanding washing was observed) and, (ii) a piece of unground paste positioned at the grid hole that was also thoroughly rinsed in distilled water and ethanol. The coating on the grid surface of the

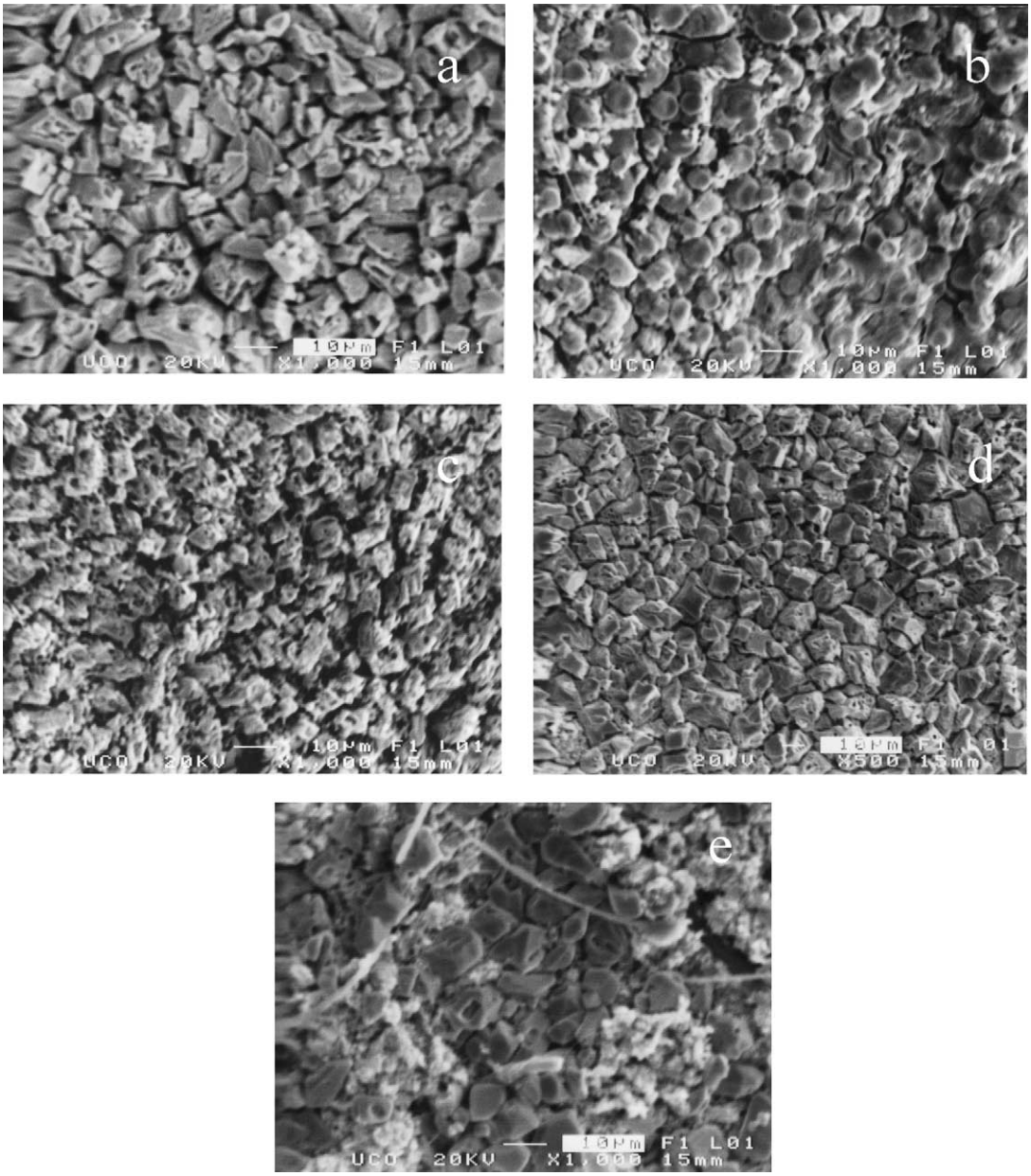

Fig. 9. SEM images of an electrode after cycling at 100% DOD. Grid surface after the fifth cycle: (a) electrode after discharge; (b, c) electrode after charge. Grid surface after the 10th cycle: (d) grid surface after charge, (e) paste after charge.

plate discharged at 100% DOD, fifth cycle (Fig. 9a) consisted of regular, well-defined particles of pseudo-prismatic morphology typical of $PbSO_4$. Similar particles were also the predominant components of the paste. The grid surface belonging to the charged plate exhibited a more complex morphology, however. Thus, there were regions where the coating consisted of pseudo-round particles of ca. 4–5 μm identified as PbO_2 particles (Fig. 9b). The coatings of other zones consisted of particles of variable morphology that resembled that of $PbSO_4$ (see Fig. 9c). The diversity in coating morphology was also present in the paste, where zones with a high concentration of $PbSO_4$ particles coexist with areas of smaller particles of ill-defined shape and probably associated with the PbO_2 phase. The presence of large (>10 μm) particles of $PbSO_4$ on the grid surface was a common occurrence in the positive plate at the 10th cycle at 100% DOD, both in discharged and in charged plates (by way of example, Fig. 9d shows the coating morphology for the charged plate). Also, the paste was found to be more homogeneous (the charged plate even exhibited well-defined $PbSO_4$ particles) (Fig. 9e). This finding is rather interesting because, in spite of the predominance of PbO_2 inferred from the X-ray and chemical analysis data (Table 3) the minor phase ($PbSO_4$) was clearly identified in the SEM images. The reason is its tendency to appearing on the paste surface by effect of its forming at the active material–electrolyte interface.

The SEM images for the cells discharged to 60% DOD revealed significant changes relative to 100% DOD. At the 10th cycle, the coating of the charged plate (Fig. 10a) consisted mainly of submicronic particles of round shape that were identified as PbO_2 particles. Also, submicronic square or pseudo-prismatic particles were observed in the discharged plates the composition of which must be $PbSO_4$. This image contrasts with that of the formed plate, Fig. 2c, and simply reflects the growth of the corrosion layer and the improved adherence between the active material and grid upon cycling. The active material exhibited similar characteristics, namely: the presence of small particles (particularly of PbO_2). The discharged plate exhibited a change in coating morphology (Fig. 10b). As in the discharged plate at 100% DOD (Fig. 9d), particle shape was clearly consistent with that of $PbSO_4$, but particle size was much smaller.

The above-described images provide a suitable model to account for the PCL of the cells cycled at 100% discharge and the capacity retention upon extensive cycling if DOD is restricted to 60%. Under the former regime, as cycling progresses, a rapid growth of $PbSO_4$ particles is observed that gives rise to a compact insulating layer at the active material/grid interface. This layer, formed by $PbSO_4$ particles several microns thick, is also observed on the paste surface and prevails beyond the fifth cycle. Although the conversion of $PbSO_4$ into PbO_2 alters the particle morphology, the increased particle size is retained. The insulating layer reduces the exchange of electrons and detracts from the reversibility of the electrochemical system. As a result, the capacity loss increases at a higher rate and a 80% drop in discharge capacity relative to the initial value occurs between the fifth and 10th cycles. By contrast, with a discharge regime of 60%, particles retain a submicronic size in the forward and reverse reactions, and the cell behaves as a reversible electrochemical system. Under these conditions, the cell preserves its delivered capacity upon extensive cycling.

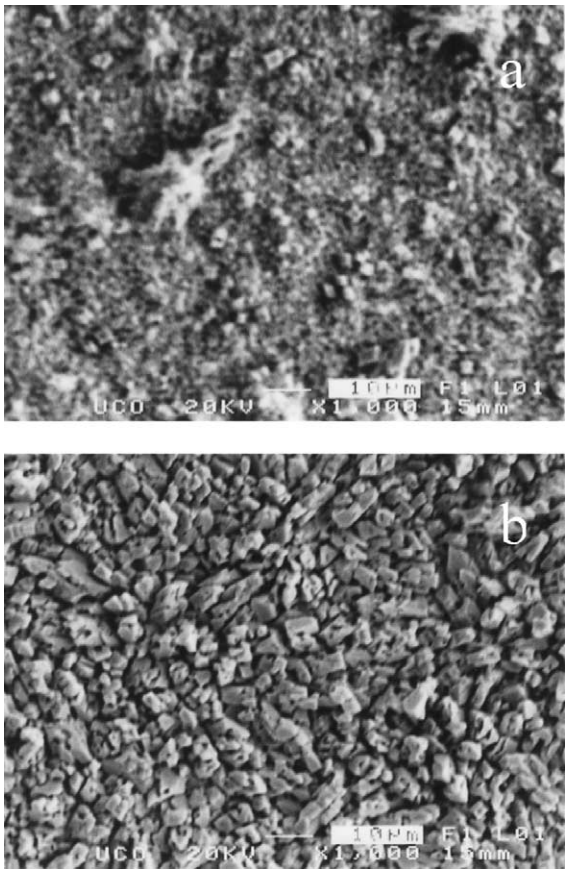

Fig. 10. SEM images of an electrode cycled at 60% DOD, 10th cycle. The images correspond to the grid surface: (a) after charge, and (b) after discharge.

3.2. Influence of curing conditions on battery life

One of the main sources of capacity fading in the lead-acid battery seems to be the lack of adherence of PAM to the substrate. The curing process creates a strong, well-defined corrosion layer at the PAM/grid interface. This corrosion layer plays a key role in the life cycle of the battery as it helps connect the grid and the active material. The curing process is affected by at least two variables, namely, the curing time and the temperature. So far, we have examined the influence of the former parameter on the electrochemical response of these thin electrodes. The curing period was extended to 4, 6, and 12 days. The cycling properties of these electrodes are shown in Fig. 11. The best results were obtained at 6 days. The cell made with the electrodes subjected to this treatment withstood more than 100 cycles. The gradual increase in cell life must reflect improved adherence of the

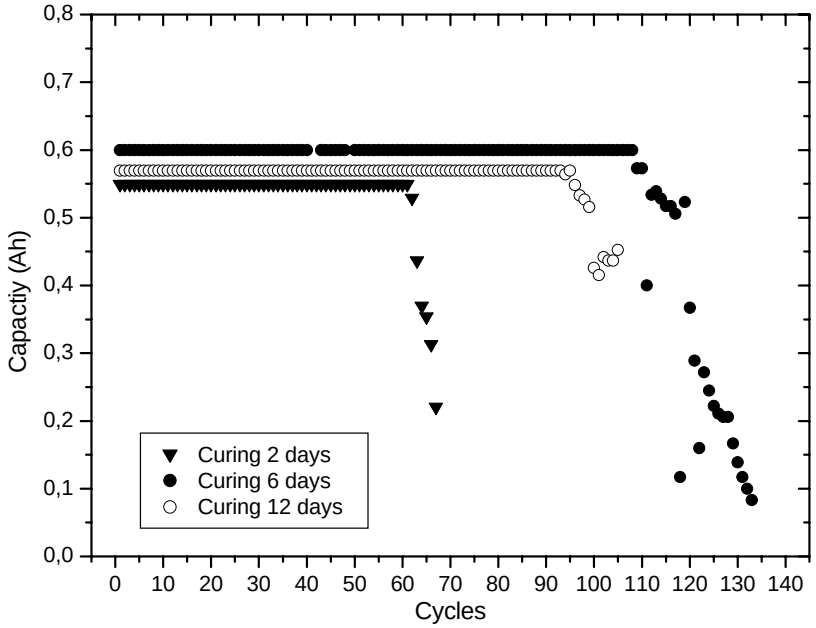

Fig. 11. Influence of the curing time on the cycling properties of the electrodes.

particles to the substrate. It seems plausible that a moderate increase in the curing time may result in the corrosion layer formed between the active material and the grid developing to a greater extent, thus favoring charge transfer at the active particle/grid interface. In fact, the degree of conversion at the formation step was also improved. A exceedingly curing period (e.g. 12 days) can give rise to a too thick corrosion layer and hence to a shortened cell life. The plates cured for 6 days at 55 °C and a relative humidity of 98% also yielded the best power capacity for the cells, (see Fig. 12). The general trend observed was a decrease in delivered energy as the power was increased. Under these curing conditions, however, the cell with the electrode cured for 6 days combined maximal power and an acceptable amount of delivered energy.

This description does not consider stratification of the electrolyte even though all measurements were performed with no agitation of the electrolyte. An increased

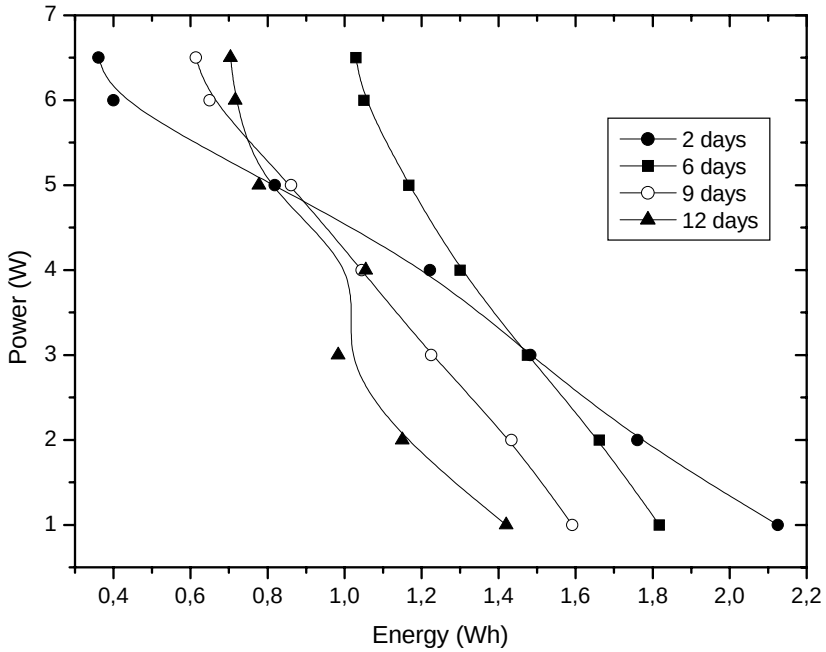

Fig. 12. Plot of the battery power vs. energy of 2 V cells with electrodes cured for variable lengths of time.

concentration of sulfuric acid at the bottom of cycled cells, which might have contributed to the capacity loss at the later cycling stages, cannot be discarded. A study of the influence of this phenomenon and other factors affecting electrode performance is currently under way in our laboratory, the results of which will be reported in future publications.

4. Conclusions

Thin plates constitute one of the major future strategies with a view to maintaining the leading positions of lead-acid batteries against emergent electrochemical energy systems. The results of this study show that, with the aid of a special device, plates of controlled, reduced thickness can be manufactured. In fact, electrodes prepared on Pb–Sn–Ca rolled grids and cycled according IEC 896-2 specification exhibited a good capacity retention at 60% DOD. Submicronic active particles form a compact coating firmly bound to the grid surface that affords the exchange of electrons at the active material/grid interface. Under these conditions, the $PbO_2 \Leftrightarrow PbSO_4$ transformation is highly reversible and the capacity delivered by the cell is maintained over a large number of cycles, especially if the plate is subjected to prolonged curing (6 days at 55 °C and a relative humidity of 98%). With deeper discharges (up to 100% DOD), a premature capacity loss in the cell was observed as a result of the irreversible transformation of the PAM into large lead sulfate crystals that deposited onto the grid surface.

Acknowledgements

This work was supported by EU contract ENK6-CT-2000-00078. We also acknowledge the assistance of the R&D Centre of Tudor (Exide Technologies), particularly from Drs. M.L. Soria and J. Valenciano.

References

[1] T.J. Juergens, US Patent 5,198,313 (1993).
[2] R.C. Bhardwaj, J. Power Sources 78 (1999) 130–138.
[3] R.C. Bhardwaj, J. Than, J. Power Sources 91 (2000) 51–61.
[4] M.L. Soria, J. Valenciano, A. Ojeda, G. Raybaut, K. Ihmels, J. Deiter, N. Clement, J. Morales, L. Sánchez, J. Power Sources 116 (2003) 61–72.
[5] R.D. Prengaman, J. Power Sources 95 (2001) 224–233.
[6] P.T. Moseley, R.D. Prengaman, J. Power Sources 107 (2002) 240–244.
[7] J.S. Chen, J. Power Sources 91 (2000) 172–177.
[8] R.J. Hill, I.C. Madsen, J. Electrochem. Soc. 131 (1984) 1486.
[9] Powder Diffraction Files, Numbers 5-561 and 37-517.
[10] S. Abaci, K. Pekmez, T. Hökelek, A. Yildiz, J. Power Sources 88 (2000) 232.
[11] D. Pavlov, G. Petkova, J. Electrochem. Soc. 149 (2002) A644–A653.